Scripta Materialia 150 (2018) 87–91

Contents lists available at ScienceDirect

Scripta Materialia

journal homepage: www.elsevier.com/locate/scriptamat

Regular article

Twinning behavior in a rolled Mg-Al-Zn alloy under dynamic impact loading

Longhui Mao [a], Chuming Liu [a,b], Tao Chen [a], Yonghao Gao [a,*], Shunong Jiang [a], Renke Wang [a]

[a] School of Materials Science and Engineering, Central South University, Changsha 410083, China
[b] School of Materials Science and Engineering, Hunan University of Science and Technology, Xiangtan 411201, China

ARTICLE INFO

Article history:
Received 19 January 2018
Received in revised form 28 February 2018
Accepted 2 March 2018
Available online xxxx

Keywords:
Twinning
Dynamic impact loading
Finite element analysis
EBSD
Magnesium alloy

ABSTRACT

Twinning-stress correlation of a basal textured Mg-Al-Zn alloy was studied after impact test. The deformed microstructure was characterized using electron backscattered diffraction (EBSD) while the stress analysis during impact process was modeled by finite element method. Results showed that both the tension and compression region of the sample were dominated by high density deformation twins. Various twinning modes and variant selections were determined by trace method and misorientation analysis. Preliminary analysis suggested that some rare twinning modes such as $\{10\bar{1}1\}$-$\{10\bar{1}1\}$ and $\{10\bar{1}2\}$-$\{10\bar{1}2\}$ double twinning likely occurred after deformation.

Due to the limited number of independent slip systems in hexagonal close-packed structure, twinning plays an important role in plastic deformation for magnesium alloys, especially at high strain rate and/or low temperature [1–4]. Among them, $\{10\bar{1}2\}$ tension, $\{10\bar{1}1\}$ compression and $\{10\bar{1}1\}$-$\{10\bar{1}2\}$ double twinning were three most frequently reported twinning modes [4–6], in increasing order of activation difficulty. Different from that of slip, the activation of twinning is sensitive to the loading direction with respect to the *c*-axis of the initial grain due to its polar nature [2]. For example, $\{10\bar{1}2\}$ twinning is prevalent by extension of the *c*-axis, while $\{10\bar{1}1\}$ twinning tends to be activated when the *c*-axis is contracted. Moreover, apart from the ability to accommodate the shear strain along *c*-axis, twins can introduce a rapid lattice reorientation, which provides feasible options to modify the texture, and furthering affects the formability, anisotropy as well as mechanical property of Mg alloy [7–9]. Hence, it is significant to assess the stress state during deformation to analyze the twinning behavior.

Over recent decades, the understanding of twinning and relevant mechanical response has been greatly enhanced with the development of EBSD technique. Considerable attentions were focused on the twinning behaviors under specified loading conditions where the certain twin modes could be produced [9–11]. However, as structural materials used in transportation vehicle, magnesium alloys usually suffer dynamic impact loading during service, which the high strain rate and severe deformation would induce more complex changes in microstructures. Additional twinning modes such as $\{10\bar{1}2\}$-$\{10\bar{1}1\}$, $\{10\bar{1}2\}$-$\{10\bar{1}2\}$ double twinning as well as some specific orientations which do not satisfy the typical twin/matrix orientation relationship have been detected in the severe deformed magnesium alloys [12–16]. Shi et al. [13] observed boundaries with orientation relationship of $78.3°/\langle 10\bar{1}2\rangle$ in Mg-Gd-Y-Zr alloy after ballistic impact. Li et al. [14] reported a twin-like domain having the misorientation of $57°/\langle 10\bar{1}0\rangle$ in the ruptured pure Mg. Despite above efforts, mechanisms about these abnormal orientations and detailed twinning characteristics (e.g. variant selection) are not clearly clarified.

Our present work aims to analyze the twinning behaviors coupled with stress distribution of AZ80 alloy under dynamic impact loading at ambient temperature. Possible mechanisms for the twin-like domains with misorientations around $55–60°/\langle 10\bar{1}0\rangle$, $68–72°/\langle 11\bar{2}0\rangle$ and $77–81°/\langle 11\bar{2}0\rangle$ are reviewed.

A hot ring rolled AZ80 alloy (Mg-8.10Al-0.46Zn-0.18Mn-0.18Ag in wt%) was used in the present study. The as-received material was solution treated at 415 °C for 2 h and then water quenched. Standard unnotched specimens with dimensions of $10 \times 10 \times 55$ mm^3 were adopted for the Charpy test. The impact velocity was ~5.23 m/s. All the specimens were prepared from the center of the rolled ring with their longitudinal direction along the rolling direction (RD) while the impact loading direction was parallel to the normal direction (ND). Microstructure and texture information were acquired using Sirion200 scanning electron microscope equipped with EBSD analysis system (HKL Channel 5). Samples for EBSD measurement were prepared following a procedure as described in [17].

* Corresponding author.
E-mail address: yonghaogao@gmail.com (Y. Gao).

https://doi.org/10.1016/j.scriptamat.2018.03.005
1359-6462/

Charpy impact test was simulated based on the experimental data obtained from tensile test, using the multi-linear isotropic hardening model embedded in ABAQUS. Corresponding tensile curve is displayed in the Supplementary section. Young's Modulus, Poisson's ratio and density of the material are 43.5 GPa, 0.34 and 1.81 g/cm^3, respectively. The yield stress is 196 Mpa. Specific boundary conditions were defined to match the experimental test, which the nodes of supporting anvils were assured to be rigid and immovable while the impact loading was constrained along normal direction during deformation. Meanwhile, the model dimensions and impact velocity were adopted in conformity to the experimental condition. Besides, to improve calculation accuracy, the meshing size in the region contacted with anvils and pendulum was refined to 50 μm while that of the rest part was 100 μm.

Fig. 1a shows the inverse pole figure (IPF) map of the solution sample. Low angle grain boundaries (LAGBs) with misorientation angles of 3–15° and high angle grain boundaries (HAGBs) with misorientation angles of 15–90° are highlighted in white and black, respectively. As can be seen, the material exhibits an equaxied microstructure with the presence of few LAGBs. Detailed analysis of the misorientation angle distribution (Fig. 1b) also verifies the result that the fraction of misorientation angle below 15° is rather small. Furthermore, only one wide peak around 30° about $\langle 11\bar{2}0 \rangle$ axis appears in this state. Fig. 1c and d present the pole figures for $\{0001\}$ and $\{10\bar{1}0\}$ plane, respectively. It reveals that the material has a typical basal texture with the $\{0001\}$ planes almost vertical to ND. Meanwhile, the six symmetrical intensity peaks shown in $\{10\bar{1}0\}$ pole figure suggests that the orientation state of the grains' ⟨a⟩ axis is inclined to be uniform. Hence, it can be inferred that the as-rolled microstructure has been homogenized after solution treatment.

The numerical model and quantitative stress distribution within the specimen are demonstrated in Fig. 2. As Fig. 2b shows, the stress is highly concentrated at the mid-span of the specimen during the impact test. Similar to three-point bending [18,19], the stress of the impact specimen transits continuously from compression on the top end (side A) that contacted with the pendulum to tension on the bottom end (side B), which would cause diverse deformation responses in different position. Fig. 2c presents the stress distribution along the impact direction near the fracture region. Apparently, both the tensile and compress stress increase as the distance to the neutral plane (zero stress plane) increases and meanwhile the stress of side A is higher than side B. Note that neutral plane has slightly tilted to the compression zone. Similar stress asymmetric phenomenon was also reported by Avedesian [19], who found that Mg alloy shortened during bending as the neutral axis deviated from the geometrical center line and moved to the tension zone. J.C. Baird et al. [18] pointed out that the neutral axis deviation varied with alloy type and loading condition. Therefore, it should be analyzed in specific case.

To further study the microstructural evolution associated with the stress state variation during test, EBSD scans near the fracture edge of the compression and tension zone, i.e. side A and side B, are shown in Fig. 3. Boundaries with different characteristic misorientation are highlighted by different colors in the image quality maps. Different from the low velocity bending microstructure [18], the impact sample experiences much heavier twinning because insufficient independent slip systems operate to accommodate the large strain in such short time. Various twin patterns, such as parallel twins and twin-twin intersections within a grain as well as zonal shape twin bands across boundaries could be observed. Barnett et al. [6] suggested that the localized shear bands could evolve from $\{10\bar{1}1\}$-$\{10\bar{1}2\}$ double twins since the doubly twinned structure contained high local shear strains. Compared to the initial microstructure, the IPF color distribution becomes rather inhomogeneous after deformation. Such orientation gradients are closely related to the lattice rotation induced by the local strains. To coordinate the lattice curvature, amounts of dislocations are required [13,20]. Once these dislocations accumulate within the deformed structure, profuse LAGBs will generate as shown in Fig. 3a and c.

In Fig. 3b, it can be seen that 86°/$\langle 11\bar{2}0 \rangle$ and 38°/$\langle 11\bar{2}0 \rangle$ boundaries (±4° offset) are most frequently observed, indicating $\{10\bar{1}2\}$ tension

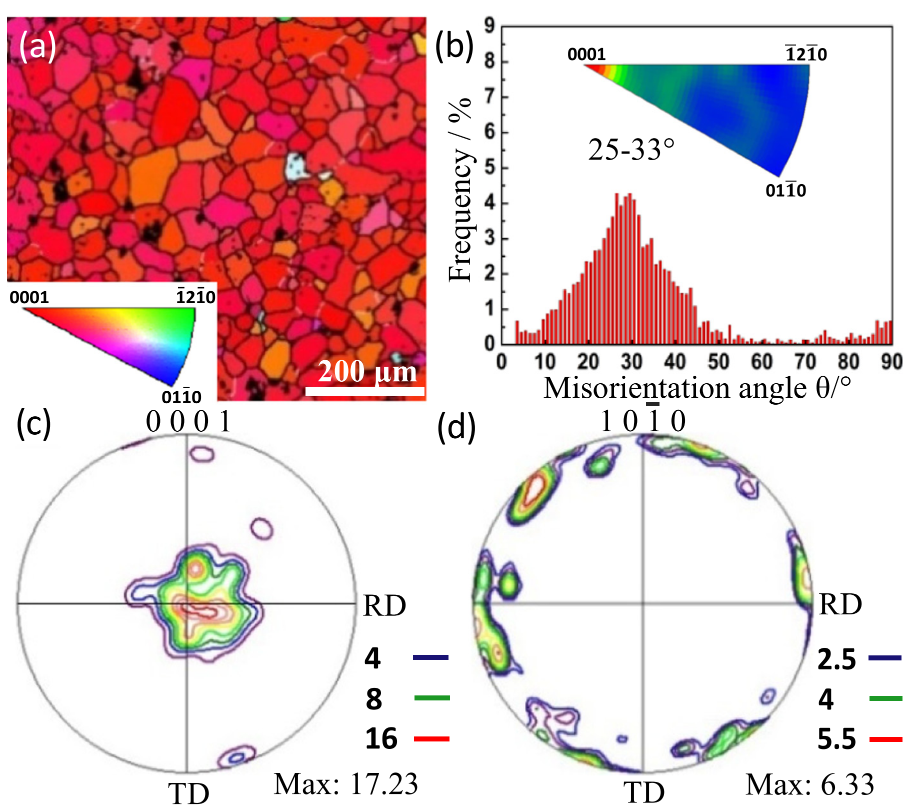

Fig. 1. Microstructure and texture of the solution sample: (a) EBSD map; (b) misorientation angle distribution map; (c) $\{0001\}$ and (d) $\{10\bar{1}0\}$ pole figure.